TENMAK BOREN BOR ARAŞTIRMA ENSTİTÜSÜ

BOR DERGİSİ
JOURNAL OF BORON
https://dergipark.org.tr/boron

Thermal decomposition behaviors, kinetics and thermodynamics of colemanite

Sevgi Polat [1,*]

[1]*Marmara University, Faculty of Engineering, Department of Chemical Engineering, İstanbul, 34722, Türkiye*

ARTICLE INFO

Article History:
Received March 14, 2024
Accepted July 14, 2024
Available online September 30, 2024

Research Article

DOI: 10.30728/boron.1452576

Keywords:
Colemanite
Morphology
Thermal kinetics
Thermodynamics

ABSTRACT

Colemanite, the most significant commercially available borate mineral with calcium content, exhibits versatile applications and is widely used in glass, textiles, ceramics, detergents, and other industries. Investigating the dehydration characteristics, kinetics, and thermodynamics of this borate mineral is important to improve its performance because of its usage in different industries. This study involves a combination of characterization and thermal dehydration kinetics of colemanite results. First, colemanite is analyzed structurally and morphologically through X-ray diffraction (XRD), Fourier transform infrared spectroscopy (FTIR), and scanning electron microscopy (SEM). Then, different heating rates were applied to investigate the thermal behavior of the colemanite using thermogravimetric analysis (TGA). Based on the obtained thermograms, the dehydration zone was selected for kinetic and thermodynamic analysis using conversional kinetic methods. The average activation energies were calculated as 64.1±4.3, 59.6±3.9, 59.9±3.7, and 60.0±4.1 kJ/mol for Flynn-Wall-Ozawa, Kissinger-Akahira-Sunose, Starink, and Tang models, respectively. Through the thermodynamic analysis, it was found that the dehydration of colemanite was a non-spontaneous and endothermic process.

1. Introduction

Türkiye is one of the top producers of borates worldwide and about 70% of the world's boron ore reserves are located in the country [1-3]. Boron is not found in nature in a free state; instead, it is usually found combined with oxygen or within other compounds, including sodium, calcium, and magnesium. The most important boron minerals are ulexite, colemanite, probertite, tincal, and kernite. Among these minerals, colemanite ($2CaO{\cdot}3B_2O_3{\cdot}5H_2O$) is the most important commercial borate mineral and raw colemanite ore contains between 28% and 42% B_2O_3 [4,5]. Colemanite is widely used in the glass, ceramics, paint, detergents industries, and nuclear fields. However, colemanite is challenging to employ directly for some industrial applications, such as in glasses and ceramics, due to its water content, which can affect the properties of the end products [6-8]. The water that occurs due to crystallization can be removed from the hydrated mineral for various technological and economic applications. For example, dehydration can benefit device design while reducing the mass of the material, which brings economic advantage through decreased transportation costs. Colemanite can be dehydrated to obtain various boron products in different forms [5,9]. Therefore, understanding the dehydration characteristics of colemanite and identifying the kinetic parameters are of great value for improving product quality and processing conditions. Various analytical techniques can be applied to study the thermal decomposition of colemanite, with thermogravimetric analysis (TGA) being one of the most popular and useful techniques. TGA monitors the changes in the mass of a material with increasing temperature. This provides valuable insights into the mineral's thermal degradation [10]. Isoconversional kinetic models can be used to obtain comprehensive information on the thermal degradation of colemanite. There are several reports on the thermal degradation and kinetics of the colemanite in the literature [4,11-14].

In this work, the thermal decomposition behavior of colemanite, an important boron mineral, was investigated using TGA. It was determined that the decomposition mainly occurred due to the removal of water, i.e. dehydration, and the borate degradation, i.e. dehydroxylation. The kinetics of the dehydration, which refers to the decomposition occurring in the range of 65-340°C, were investigated using different isoconversional models. The novelty of the presented paper is, combining kinetic and thermodynamics calculations to provide a comprehensive report on the colemanite dehydration process. In addition, colemanite was subjected to structural and morphological analysis to determine the physicochemical properties.

*Corresponding author: sevgi.polat@marmara.edu.tr

2. Experimental Method

The colemanite ore sample was supplied from the Kütahya region Emet, by Eti Mine Inc. (Türkiye). The chemical analysis results indicated that it contains 39.5% B_2O_3, 26.2% CaO, 22.1% H_2O and 12.2% other oxides such as SiO_2, Na_2O, MgO and Al_2O_3. The structure of the colemanite was characterized using an X-ray diffractometer (XRD, Bruker D2 Phaser, USA) by collecting a diffraction pattern with a scanning range of 10-70° with a copper target. The X-ray generator was set at a tube voltage of 40 kV and a current of 40 mA. Attenuated total reflectance - Fourier transformed infrared (ATR-FTIR, Shimadzu IR Affinity-1, Japan) spectrum was recorded with a scanning range from 600 to 4000 cm^{-1}. The particle morphology was investigated using scanning electron microscopy (SEM, Zeiss EVO LS 10, Germany). energy dispersive spectroscopy (EDS) mapping was also recorded. The thermal property of the colemanite was observed using a TGA (Netzsch STA 409, Germany). Before the experiments, several blank experiments were conducted to obtain the baseline to use as corrections. Approximately 10 mg of the sample was accurately weighed into an aluminum pan. The sample was heated with a constant heating ramp of 5, 10, 20, and 40°C/min from 30°C to 950°C while nitrogen (N_2) was supplied at a constant flow rate (20 cm^3/min). The data collected were further analyzed for kinetic analysis. In this study, four prominent isoconversional methods, such as the Flynn-Wall-Ozawa (FWO) [15,16], Kissinger-Akahira-Sunose (KAS) [17,18], Starink [19], and Tang [20] models were utilized to conduct the dehydration kinetic parameters such as the pre-exponential factor and activation energy. The linearized forms of the kinetic models are given in Equations 1-4, respectively.

$$\text{FWO: } \ln\beta = \ln\left(\frac{AE}{Rg(x)}\right) - 5.331 - 1.052\frac{E}{RT} \quad (1)$$

$$\text{KAS: } \ln\left(\frac{\beta}{T^2}\right) = \ln\left(\frac{AR}{Eg(x)}\right) - \frac{E}{RT} \quad (2)$$

$$\text{Starink: } \ln\left(\frac{\beta}{T^{1.92}}\right) = C - 1.0008\frac{E}{RT} \quad (3)$$

$$\text{Tang: } \ln\left(\frac{\beta}{T^{1.8947}}\right) = C - 1.00145\frac{E}{RT} \quad (4)$$

where A is the pre-exponential or frequency factor (min^{-1}), E is the activation energy (kJ/mol), β is the heating rate (°C/min), T is the absolute temperature (K), R is the ideal gas constant (8.314 J/mol K). To estimate the frequency factor (A) for each value of α, Kissinger's equation [21] given in Equation 5 was used in this study.

$$A = \frac{\beta E \exp(E/RT_{peak})}{RT^2_{peak}} \quad (5)$$

Based on kinetics, thermodynamic parameters of the dehydration process, including enthalpy change (ΔH), Gibbs free energy change (ΔG), and entropy change (ΔS), can be obtained by using kinetic parameters and Eyring equations [22,23].

$$\Delta H = E - RT \quad (6)$$

$$\Delta G = E + RT_{peak}\ln\left(\frac{K_B T_{peak}}{hA}\right) \quad (7)$$

$$\Delta S = \frac{\Delta H - T\Delta G}{T_{peak}} \quad (8)$$

where T_{peak} is the peak temperature of the derivative thermogravimetry (DTG) (mass loss rate) curve, K_B is the Boltzmann constant, and h is the Planck constant.

3. Results and Discussion

3.1. Characterization

In this study, characterization was performed to investigate the structural and morphological characteristics of the colemanite. The XRD and FTIR results of the colemanite are presented in Figures 1a and 1b, respectively.

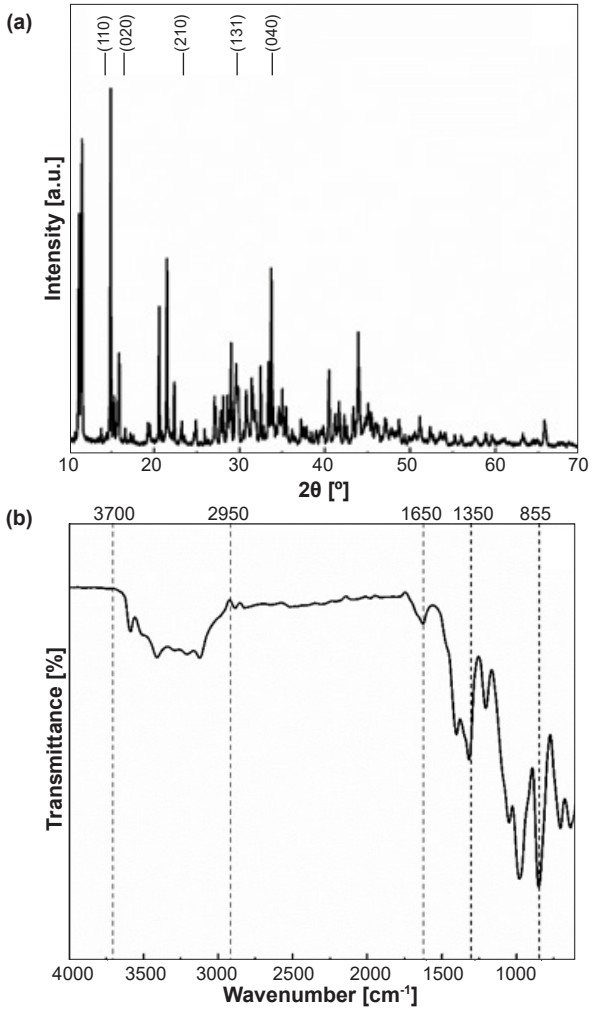

Figure 1. a) XRD pattern and b) FTIR spectrum for colemanite.

According to the XRD result, the distinct characteristic diffraction peaks were determined at 2θ of 13.28, 15.68, 22.94, 28.34, and 31.67° and corresponded to the (110), (020), (210), (131), and (040) lattice planes of the colemanite, respectively. These peaks align with the positions of the colemanite diffraction standard

card (ICDD PDF No: 33-0267), confirming the structure of colemanite. The crystal system was a monoclinic structure, and the unit cell parameters were calculated using the Rietveld refinement method as a=8.751 Å, b=11.292 Å, c=6.146 Å, and β=109.56°, consistent with those reported in earlier studies [7,8]. FTIR analysis was conducted to determine functional groups in the colemanite. Figure 1b shows the typical characteristic FTIR absorption bands of colemanite. The broad peak between 3700 and 2950 cm^{-1} is associated with the stretching hydroxyl groups in the structure, and the small peak at about 1630 cm^{-1} is attributed to the H-O-H (lattice water) [24]. The asymmetric stretching vibrations of B_3-O are associated with the peak at 1459 cm^{-1} and 1354 cm^{-1}. The peaks at 1317 and 1210 cm^{-1} are connected to the bending vibrational modes of the B-OH. Furthermore, the peaks at 1047 and 855 cm^{-1} are linked to the asymmetric and symmetric stretching of $B_{(4)}$-O, respectively [8,25]. FTIR spectrum supported the finding of the XRD result and confirmed the presence of colemanite.

Figure 2 displays the SEM image of the colemanite with the EDS result. When the SEM image of the colemanite mineral was examined, it was observed that both small and large particles coexisted. As consistent with the literature [9,26], the size and morphology of the particles were not homogeneous, and the surfaces were rough. Individual smaller particles identified in the SEM image had ~4 µm size. These small particles combined to form larger particles and the particles had an intense agglomeration tendency. Furthermore, the EDS spectrum confirmed the presence of Ca and O elements, which are constituents of colemanite.

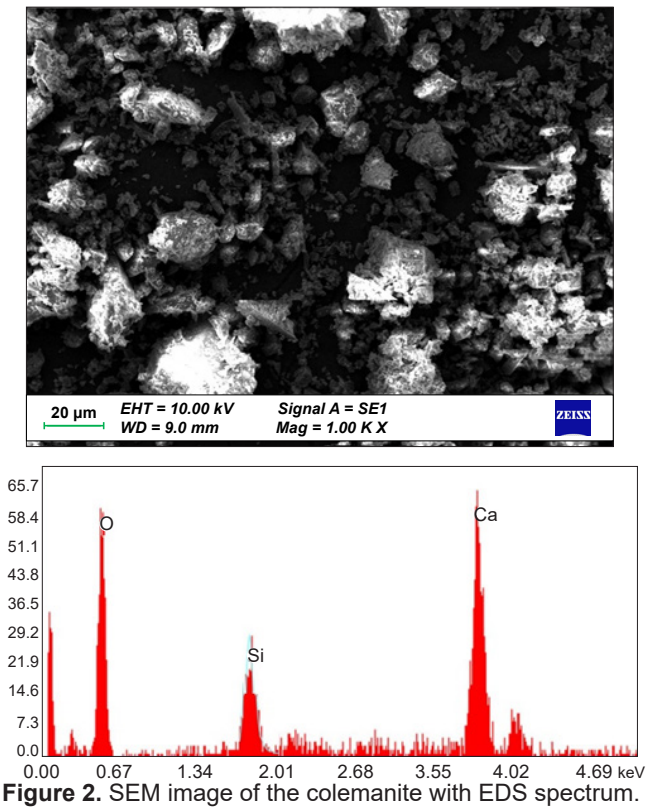

Figure 2. SEM image of the colemanite with EDS spectrum.

3.2. Thermal Analysis

The thermal decomposition characteristics of colemanite play a crucial role in using high-temperature process applications. Therefore, thermal analysis was performed at different heating rates. Figures 3a and 3b present the TGA and DTG curves for colemanite at heating rates of 5, 10, 20, and 30°C/min.

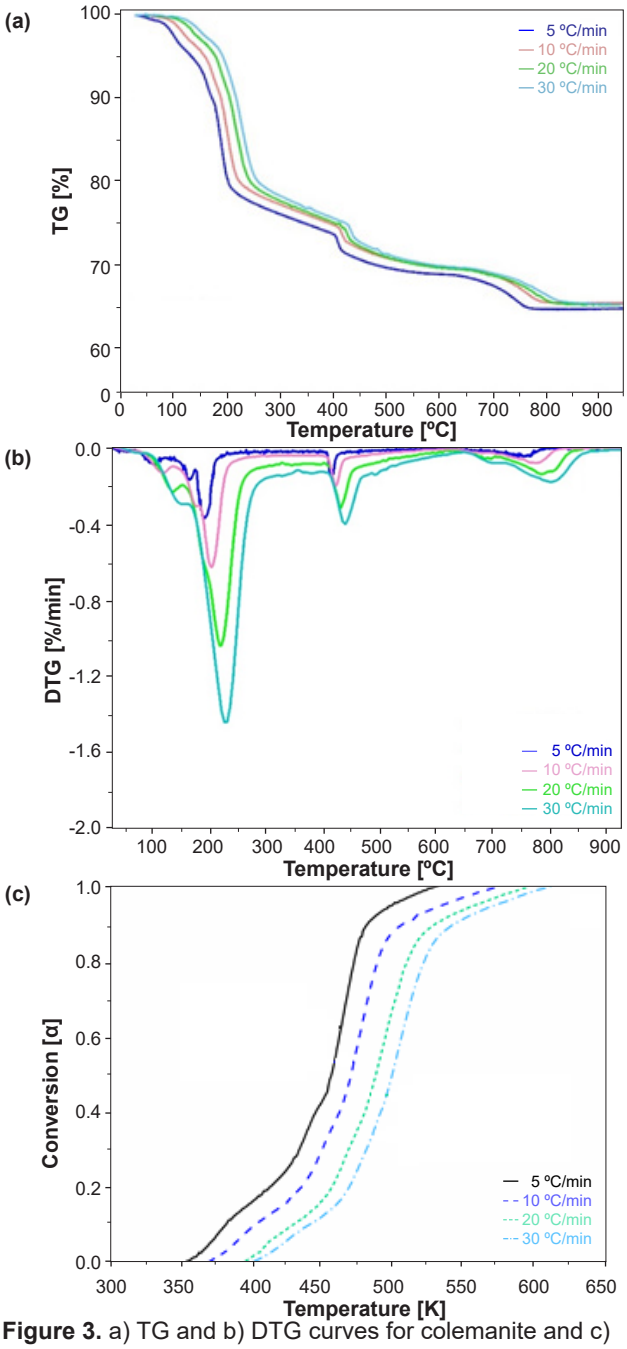

Figure 3. a) TG and b) DTG curves for colemanite and c) Conversion vs. temperature for colemanite dehydration at 5, 10, 20, and 30°C/min.

The DTG curve exhibited a three-step mass loss. Considering the first loss in mass, i.e. the complete dehydration of colemanite, the total theoretical mass loss should be 21.89% as shown in the following equation:

$$2CaO.3B_2O_3.5H_2O \rightarrow Ca_2B_6O_{11} + 5H_2O \quad (9)$$

The TGA curves reveal a mass loss of ~22% within the temperature range of 65 to 340°C, which closely matches the theoretical value of crystalline water content for colemanite. As shown in the DTG curves, the maximum mass loss rate of colemanite occurred at 191°C, 197°C, 219°C, and 231°C for 5, 10, 20, and 30°C/min, respectively. According to the TGA and DTG results, increasing the heating rate from 5 to 40°C, the peak temperature moved towards the higher temperature due to the thermal lag effect. Moreover, the DTG curves display two additional peaks at higher temperatures. The second loss in mass is approximately 5% with an onset temperature of ~380°C and finishing at ~600°C and it can be associated with the calcite decomposition according to the following equation:

$$CaCO_3 \rightarrow CaO + CO_2 \quad (10)$$

A third mass loss event occurs between ~650°C and ~900°C as stated in the literature, this peak may arise from the recrystallization of the subsequent amorphous phase [1].

3.3. Kinetic and Thermodynamic Analysis

In this study, the dehydration kinetics of colemanite minerals were examined. Therefore, kinetic and thermodynamic calculations were made using TGA data in the 65-340°C range using four different kinetic models, namely FWO, KAS, Starink, and Tang models. Figure 3c illustrates the conversion degree (α) versus temperature in the dehydration zone for different heating rates.

The conversion degree (α) is defined as:

$$\alpha = W_0 - W_t / W_0 - W_f \quad (11)$$

where W_0, W_t, and W_f refer to the initial, instantaneous mass at time t and final sample mass, respectively. Using this data, the plots for FWO, KAS, Starink, and Tang models were obtained at various extents of conversions from 0.1 to 0.9, and the results are given in Figure 4.

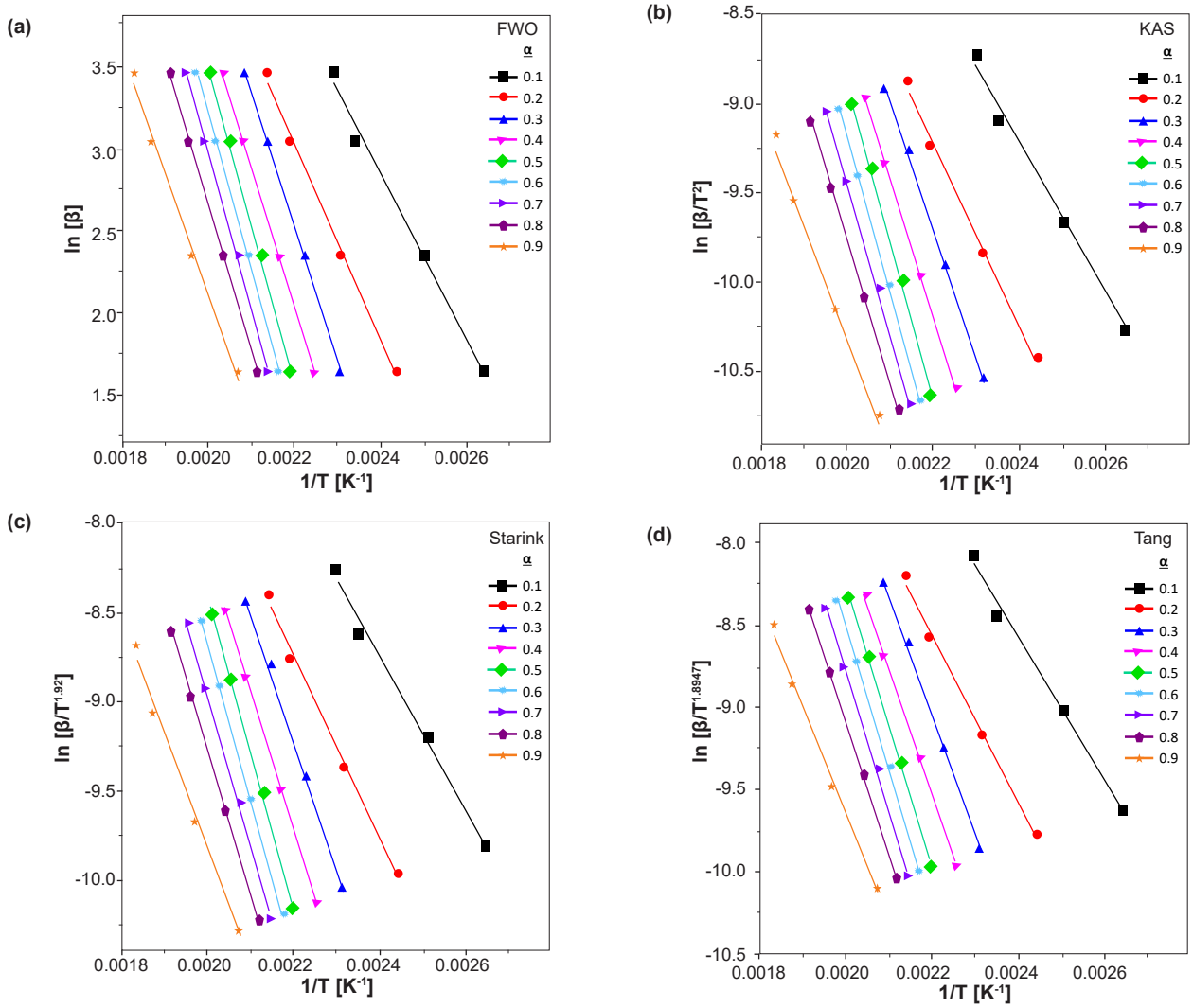

Figure 4. Linear fit plots to calculate activation energy for colemanite.

Activation energies, minimum energy needed for the reaction, and the corresponding correlation coefficients were calculated using the slopes of each line. Figure 5 shows the activation energy values at different conversion degrees determined by different kinetic models.

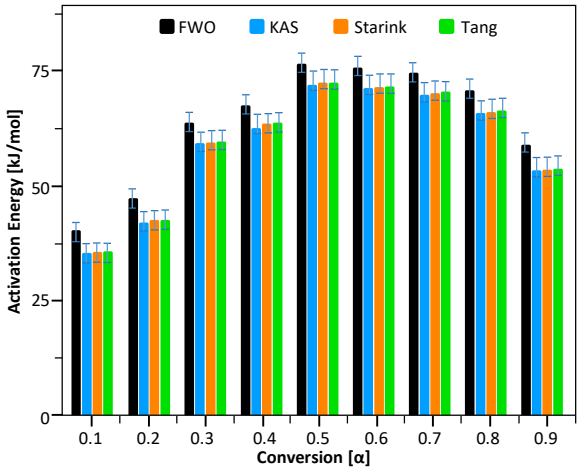

Figure 5. Activation energy with respect to conversion degree for colemanite.

All correlation coefficients of fitted models to the experimental data were higher than 0.95, showing the model agreed with the experimental results and indicating its suitability for accurately describing dehydration. The activation energies and pre-exponential factors obtained by different models range from 35.6 to 76.1 kJ/mol and 1.77×10^3 to 1.46×10^8 min, respectively. The fluctuation tendency of the four kinetic models was similar, and the activation energy of the colemanite during thermal decomposition was increased as dehydration started, then decreased slightly in a conversion degree between 0.6 and 0.9. This fluctuation indicated that the activation energy varied depending on the conversion degree. The average activation energies of colemanite were 64.1±4.3, 59.6±3.9, 59.9±3.7, and 60.0±4.1 kJ/mol for FWO, KAS, Starink, and Tang models, respectively. It was found that there were small discrepancies between the calculated activation energies from different models due to the different approximations on which the used models are based. Waclawska [12] calculated the activation energy ranges of 393.7-102.6 J/g depending on the grinding time for the colemanite dehydration process.

Based on the activation energies, thermodynamic parameters of colemanite were calculated for 10°C/min, and the results were listed in Table 1.

Table 1. Thermodynamic parameters for thermal decomposition of colemanite at 10°C/min.

α	FWO				KAS			
	A (min^{-1})	ΔH (kJ/mol)	ΔG (kJ/mol)	ΔS (kJ/mol)	A (min^{-1})	ΔH (kJ/mol)	ΔG (kJ/mol)	ΔS (kJ/mol)
0.1	6.60×10^3	36.4	122.9	-183.9	1.77×10^3	31.7	123.3	-194.8
0.2	4.74×10^4	43.5	122.2	-167.5	1.24×10^4	38.7	122.6	-178.6
0.3	4.58×10^6	60.2	121.0	-129.5	1.45×10^6	55.9	121.3	-139.1
0.4	1.26×10^7	63.9	120.8	-121.1	4.00×10^6	59.6	121.1	-130.6
0.5	1.46×10^8	73.0	120.3	-100.7	5.06×10^7	69.0	120.5	-109.5
0.6	1.17×10^8	72.2	120.4	-102.5	3.92×10^7	68.1	120.6	-111.6
0.7	7.77×10^7	70.6	120.5	-106.0	2.47×10^7	66.4	120.7	-115.5
0.8	2.86×10^7	66.9	120.7	-114.3	8.32×10^6	62.4	120.9	-124.5
0.9	1.20×10^6	55.2	121.4	-140.7	2.71×10^5	49.8	121.7	-153.0
Av.	**4.64×10^6**	**60.2**	**121.1**	**-129.6**	**1.43×10^7**	**55.7**	**121.4**	**-139.7**
α	Starink				Tang			
	A (min^{-1})	ΔH (kJ/mol)	ΔG (kJ/mol)	ΔS (kJ/mol)	A (min^{-1})	ΔH (kJ/mol)	ΔG (kJ/mol)	ΔS (kJ/mol)
0.1	1.89×10^3	32.0	123.3	-194.3	1.93×10^3	32.0	123.3	-194.1
0.2	1.34×10^4	38.9	122.6	-178.0	1.36×10^4	39.0	122.6	-177.9
0.3	1.55×10^6	56.2	121.3	-138.5	1.57×10^6	56.2	121.3	-138.4
0.4	4.29×10^6	59.9	121.1	-130.0	4.35×10^6	60.0	121.1	-129.9
0.5	5.43×10^7	69.3	120.5	-108.9	5.50×10^7	69.4	120.5	-108.8
0.6	4.21×10^7	68.4	120.6	-111.1	4.27×10^7	68.4	120.6	-110.9
0.7	2.65×10^7	66.6	120.7	-114.9	2.69×10^7	66.7	120.7	-114.8
0.8	8.97×10^6	62.6	120.9	-123.9	9.11×10^6	62.7	120.9	-123.8
0.9	2.93×10^5	50.1	121.7	-152.3	2.99×10^5	50.2	121.7	-152.2
Av.	**1.53×10^7**	**56.0**	**121.4**	**-139.1**	**1.55×10^7**	**56.1**	**121.4**	**-139.0**

As seen in Table 1, the decomposition of colemanite exhibited a positive value for ΔH, indicative that the reaction was an endothermic process. The ΔG represented the increase in total energy in a system and was a comprehensive evaluation of heat and disorder. As shown in Table 1, the ΔG values of colemanite were between 120.3 and 123.3 kJ/mol for different kinetic models. The ΔG values displayed positive, suggesting a non-spontaneous reaction that necessitated external energy input to facilitate the process. The degree of disorder within the dehydration system is measured by ΔS. The decomposition of colemanite resulted in negative ΔS values, indicating a decrease in disorder.

4. Conclusions

The current study focused on the investigation of the thermal decomposition behaviors, kinetics, and thermodynamics of colemanite minerals. XRD result demonstrated that the crystal system was a monoclinic structure. The kinetics and thermodynamics of colemanite were determined by TGA. The value of average activation energy was 64.1±4.3 kJ/mol, and the average pre-exponential factor was 4.64×10^{6} min^{-1} using for FWO model. The results of the other three isoconversional models used were compatible with FWO. The ΔH, ΔG, and ΔS for the colemanite varied between 31.7 and 73.0 kJ/mol, 120.3 and 123.3 kJ/mol, and -100.7 and -194.8 J/mol.K depending on the kinetic model at 10°C/min, respectively. It is believed that this study will provide beneficial information to better understand the thermal characteristics, kinetics, and thermodynamics of colemanite.

References

[1] Rusen, A. (2018). Investigation of structural behaviour of colemanite depending on temperature. *Revista Română de Materiale/Romanian Journal of Materials*, *48*(2), 245-251. Retrieved from https://solacolu.chim.upb.ro/p245-250.pdf

[2] Celik, A. G., & Cakal, G. O. (2016). Characterization of espey colemanite and variation of its physical properties with temperature. *Physicochemical Problems of Mineral Processing*, *52*(1), 66-76. https://doi.org/10.5277/ppmp160106

[3] Terzi, E. (2018). Thermal degradation of particleboards incorporated with colemanite and common boron-based fire retardants. *BioResources*, *13*(2), 4239-4251. https://doi.org/10.15376/biores.13.2.4239-4251

[4] Kizilca, M., & Copur, M. (2017). Thermal dehydration of colemanite: kinetics and mechanism determined using the master plots method. *Canadian Metallurgical Quarterly*, *56*(3), 259-271. https://doi.org/10.1080/00084433.2017.1349023

[5] Yıldız, Ö. (2004). The effect of heat treatment on colemanite processing: A ceramics application. *Powder Technology*, *142*, 7-12. https://doi.org/10.1016/j.powtec.2004.03.006

[6] Lotti, P., Gatta, D., Demitri, N., Guastella, G., Rizzato, S., Ortenzi, M. A., … & Fernandez-Diaz M. T. (2018). Crystal chemistry and temperature behavior of the natural hydrous borate colemanite, a mineral commodity of boron. *Physics and Chemistry of Minerals*, *45*, 405-422. https://doi.org/10.1007/s00269-017-0929-7

[7] Lotti, P., Comboni, D., Gigli, L., Carlucci, L., Mossini, E., Macerata, E., … & Gatta, G. D. (2019) Thermal stability and high-temperature behavior of the natural borate colemanite: An aggregate in radiation-shielding concretes. *Construction and Building Materials*, *203*, 679-686. https://doi.org/10.1016/j.conbuildmat.2019.01.123

[8] Frost, R. L., Scholz, R., Ruan, X., Malena, R., & Lima, F. (2016). Thermal analysis and infrared emission spectroscopy of the borate mineral colemanite (CaB3O4(OH)3H2O). *Journal of Thermal Analysis and Calorimetry*, *124*, 131-135. https://doi.org/10.1007/s10973-015-5128-5

[9] Uysal, T., Mutlu, H. S., & Erdemoğlu, M. (2016). Effects of mechanical activation of colemanite (Ca2B6O11·5H2O) on its thermal transformations. *International Journal of Mineral Processing, 151*, 51-58. https://doi.org/10.1016/j.minpro.2016.04.006

[10] Ozawa, T. (2000). Thermal analysis-review and prospect. *Thermochimica Acta*, *355*, 35-42. https://doi.org/10.1016/S0040-6031(00)00435-4

[11] Waclawska, I., Stoch, L., Paulik, J., & Paulik, F. (1988). Thermal decomposition of colemanite. *Thermochimica Acta*, *126*, 307-318. https://doi.org/10.1016/0040-6031(88)87276-9

[12] Waclawska, I. (1997). Thermal behaviour of mechanically amorphized colemanite. *Journal of Thermal Analysis*, *48*, 145-154. https://doi.org/10.1007/BF01978975

[13] Kutuk, S. (2024). Morphology, crystal structure and thermal properties of nano-sized amorphous colemanite synthesis. *Arabian Journal for Science and Engineering*, *49*, 11699-11716. https://doi.org/10.1007/s13369-024-08801-4

[14] Kalita, J. M., Kaya-Keleş, Ş., Çakal, G. Ö., Meriç N., & Polymeris, G. S. (2022) Thermoluminescence and optically stimulated luminescence of colemanite-rich borate mineral. *Journal of Luminescence*, *242*, 118580. https://doi.org/10.1016/j.jlumin.2021.118580

[15] Ozawa, T., (1965). A new method of analyzing thermogravimetric data. *Bulletin of the Chemical Society of Japan*, *38*, 1881-1886. https://doi.org/10.1246/bcsj.38.1881

[16] Flynn, J. H., & Wall, L. A. (1966). General treatment of the thermogravimetry of polymers. *Journal of Research of the National Institute of Standards and Technology*, *70*, 487-523. https://doi.org/10.6028%2Fjres.070A.043

[17] Kissinger, H. E. (1957). Reaction kinetics in differential thermal analysis. *Analytical Chemistry*, *29*, 1702-1706. https://doi.org/10.1021/ac60131a045

[18] Koga N., Vyazovkin S., Burnham A. K., Favergeon L., Muravyev N. V., Pérez-Maqueda L. A., … & Sánchez-Jiménez P. E. (2023). ICTAC Kinetics Committee recommendations for analysis of thermal decomposition kinetics. *Thermochimica Acta*, *719*, 179384. https://doi.org/10.1016/j.tca.2022.179384

[19] Starink, M. (1996). A new method for the derivation of activation energies from experiments performed at constant heating rate. *Thermochimica Acta*, *288*, 97-104. https://doi.org/10.1016/S0040-6031(96)03053-5

[20] Tang, W., Liu, Y., Zhang, H., & Wan, C., (2003). New approximate formula for Arrhenius temperature integral. Thermochimica Acta, *408*, 39-43. https://doi.org/10.1016/S0040-6031(03)00310-1

[21] Kissinger, H. (1956). Variation of peak temperature with heating rate in differential thermal analysis. *Journal of Research of the National Institute of Standards and Technology*, *7*, 217-221. http://dx.doi.org/10.6028/jres.057.026

[22] Eyring, H. (1935). The activated complex in chemical reactions. *The Journal of Chemical Physics*, *3*, 107-115. https://doi.org/10.1063/1.1749604

[23] Evans, M. G., & Polanyi, M. (1935). Some applications of the transition state method to the calculation of reaction velocities especially in solution. *Transactions of the Faraday Society*, *31*, 875-894. https://doi.org/10.1039/TF9353100875

[24] Jun, L., Shuping, X., & Shiyang, G. (1995). FT-IR and Raman spectroscopic study of hydrated borates. *Spectrochimica Acta*, *51A*, 519-532. https://doi.org/10.1016/0584-8539(94)00183-C

[25] Budak, A., & Gönen, M. (2014). Extraction of boric acid from colemanite mineral by supercritical carbon dioxide. *The Journal of Supercritical Fluids*, *92*, 183-189. https://doi.org/10.1016/j.supflu.2014.05.016

[26] Morova, N., & Terzi S. (2015). Evaluation of colemanite waste as aggregate hot mix asphalt concrete. *Suleyman Demirel University Journal of Natural and Applied Science*, *19*(2), 8-15. Retrieved from https://dergipark.org.tr/en/download/article-file/193981